



HAL
open science

Kinetic Modeling of the Photocatalytic Degradation of Chlorinated Aromatic Volatile Organic Compounds: Mass Transfer Enhancement

N'Zanon Aly Kone, Aymen Amine Assadi, Nacer Belkessa, Lotfi Khezami, Sandotin Lassina Coulibaly, Youcef Serhane, Walid Elfalleh, Lacina Coulibaly, Abdelkrim Bouzaza, Aymen Amine Assadi

► To cite this version:

N'Zanon Aly Kone, Aymen Amine Assadi, Nacer Belkessa, Lotfi Khezami, Sandotin Lassina Coulibaly, et al.. Kinetic Modeling of the Photocatalytic Degradation of Chlorinated Aromatic Volatile Organic Compounds: Mass Transfer Enhancement. Applied Sciences, 2024, Applied Sciences, 14 (4), pp.1507. 10.3390/app14041507 . hal-04479214

HAL Id: hal-04479214

<https://hal.science/hal-04479214>





Submitted on 27 Feb 2024

HAL is a multi-disciplinary open access archive for the deposit and dissemination of scientific research documents, whether they are published or not. The documents may come from teaching and research institutions in France or abroad, or from public or private research centers.

L'archive ouverte pluridisciplinaire **HAL**, est destinée au dépôt et à la diffusion de documents scientifiques de niveau recherche, publiés ou non, émanant des établissements d'enseignement et de recherche français ou étrangers, des laboratoires publics ou privés.

Article

Kinetic Modeling of the Photocatalytic Degradation of Chlorinated Aromatic Volatile Organic Compounds: Mass Transfer Enhancement

N'Zanon Aly Koné ¹, Amine Aymen Assadi ^{2,3,*}, Nacer Belkessa ³, Lotfi Khezami ⁴, Sandotin Lassina Coulibaly ¹, Youcef Serhane ³, Walid Elfalleh ⁵, Lacina Coulibaly ¹, Abdelkrim Bouzaza ³ and Abdeltif Amrane ^{3,*}

- ¹ UFR d'Ingénierie Agronomique Forestière et Environnementale, Université de Man, Man M139PL, Côte d'Ivoire; nzanonalykone352@gmail.com (N.A.K.); sandotin.coulibaly@univ-man.edu.ci (S.L.C.); coulacina2003@yahoo.fr (L.C.)
- ² College of Engineering, Imam Mohammad Ibn Saud Islamic University (IMSIU), Riyadh 11432, Saudi Arabia
- ³ École Nationale Supérieure de Chimie de Rennes, CNRS, ISCR (Institut des Sciences Chimiques de Rennes)–UMR 6226, Université Rennes, F-35000 Rennes, France; nacer.belkessa@ensc-rennes.fr (N.B.); youcef.serhane@ensc-rennes.fr (Y.S.); abdelkrim.bouzaza@ensc-rennes.fr (A.B.)
- ⁴ Chemistry Department, College of Science, Imam Mohammad Ibn Saud Islamic University (IMSIU), Riyadh 11623, Saudi Arabia; lhmkhezami@mamu.edu.sa
- ⁵ Energy, Water, Environment and Process Laboratory, National Engineering School of Gabes, University of Gabes, Gabes 6072, Tunisia; walid.elfalleh@fst.rnu.tn
- * Correspondence: ssadi@imamu.edu.sa or aymen.assadi@ensc-rennes.fr (A.A.A.); abdeltif.amrane@univ-rennes.fr (A.A.)

Abstract: Chlorobenzene (CB) and Chloronaphthalene (CN) emissions from cement plant operations pose significant environmental risks. This study investigates the mass transfer effects of chlorinated aromatic Volatile Organic Compounds (VOCs), specifically CB and CN, in the gas phase of a continuous-tangential-flow annular photocatalytic reactor. The experiments involved introducing CB and CN into the reactor, and the degradation kinetics were analyzed using the Langmuir–Hinshelwood (L-H) model. The L-H model was applied to assess the impact of the flow rate, concentration, and relative humidity (% RH) on the degradation rate (DR). The results indicate that both the experimental and simulated degradation rates improved with increased flow rates (1 to 9 m³·h⁻¹) and inlet concentrations (30 to 216 mg·m⁻³). This enhancement of the DR correlates with the availability of active OH* species on the TiO₂ surface. The L-H model emphasizes the role of H₂O molecules in VOC removal kinetics. The degradation rates increased with a rising water content (5 to 55%), but adverse effects on VOC conversion were observed beyond a 55% RH. This study reveals a mass transfer effect, with internal diffusional limitations in the TiO₂ pores under operational conditions. The kinetics were predominantly controlled by chemical kinetics and catalyst pore availability. Furthermore, this study demonstrates a higher CB degradation than CN in the reactor and experimental conditions. For a concentration of 1.328 mM·m⁻³, the CB DR ranged from 0.70 to 2.84 μM·m²·s⁻¹, as the flow rate varied from 1 to 9 m³·h⁻¹. The CN DR varied from 0.60 to 2.20 μM·m²·s⁻¹ within the same flow rate range.

Keywords: air treatment; reactor modeling; mass transfer; pilot scale; relative humidity



Citation: Koné, N.A.; Assadi, A.A.; Belkessa, N.; Khezami, L.; Coulibaly, S.L.; Serhane, Y.; Elfalleh, W.; Coulibaly, L.; Bouzaza, A.; Amrane, A. Kinetic Modeling of the Photocatalytic Degradation of Chlorinated Aromatic Volatile Organic Compounds: Mass Transfer Enhancement. *Appl. Sci.* **2024**, *14*, 1507. <https://doi.org/10.3390/app14041507>

Academic Editor: Hicham Idriss

Received: 4 January 2024

Revised: 25 January 2024

Accepted: 5 February 2024

Published: 13 February 2024



Copyright: © 2024 by the authors. Licensee MDPI, Basel, Switzerland. This article is an open access article distributed under the terms and conditions of the Creative Commons Attribution (CC BY) license (<https://creativecommons.org/licenses/by/4.0/>).

1. Introduction

Air pollution has far-reaching environmental consequences, including the acidification of rivers, soils, and the atmosphere, the eutrophication of lakes and rivers, ozone layer depletion, and intensified greenhouse effects [1–4]. Various VOCs are responsible for these nuisances, such as chlorobenzene (CB) and chloronaphthalene (CN), which are chemicals from the cement industry [5–7]. The impact of CB and CN extends beyond environmental concerns, as these chemicals pose toxicity risks to human health [6]. Notably, due to their

volatility, cement workers face potential exposure to these VOCs, presenting a significant public health challenge [8–11].

In response to these challenges, since the 1980s regulations have been established to limit the emissions of these compounds into the air, safeguarding worker health. For the good application of these rules, it is, thus, necessary to continue to propose to industrialists innovative treatment solutions adapted to these gas emissions. Consequently, research advancements in photocatalysis have revealed the efficacy of this chemical process for purifying air contaminated by VOCs through continuous reactors.

Heterogeneous photocatalysis involves the absorption of photons by a semiconductor with an energy equal to or greater than that of the band gap ($E_c - E_v$), facilitating the flow of electrons from the valence band (E_v) to the conduction band (E_c) [12,13]. This process generates a positive hole (h^+) at the valence band and releases an electron (e^-) into the conduction band [14,15]. This chemical process consists of oxidizing the pollutant on a catalyst (TiO_2 usually) under UV radiation [16–18]. In the presence of oxygen and/or water vapor, the UV radiation that activates the semiconductor (catalyst) allows for the VOCs in contact with the reactive surface to convert into CO_2 and H_2O [19–21].

Photocatalysis generally proceeds in three steps: the mass transfer of the pollutant to the catalyst, the adsorption on the catalyst, and the chemical reaction. Among continuous photocatalytic reactors, tangential flow configurations, which consider the VOC concentration, UV intensity, and water vapor composition, offer adaptability to an industrial scale [22]. The desorption and diffusion processes of VOCs and their by-products are typically negligible, and steady-state kinetic models often overlook the mass transfer effects. Thus, the adsorption of the pollutant and the oxidation reaction are usually described by the Langmuir–Hinshelwood (L-H) theory [23–26]. In this study, a continuous-tangential-flow photoreactor is employed to assess the impact of the mass transfer on the degradation of CB and CN at industrial concentrations. The investigation includes an analysis of the influence of the flow rate, concentration, and relative humidity (RH) of the air stream on the degradation rate. Additionally, a Langmuir–Hinshelwood (L-H) modeling of the experimental results is conducted.

The scientific challenge addressed in this work is to highlight the effect of chlorinated radicals on the performance of photocatalytic reactors. In fact, the novelty is based on the treatment of simulated gas air from a cement factory. The experiments were carried out on a pilot scale under conditions similar to those on site. This was done in favor of emphasizing the true photocatalytic performances. A modeling component was established to underscore the effect of the mass transfer on the removal kinetics. To the best of our knowledge, there is no existing work on these pollutants at a pilot scale.

2. Experimental Setup

The overall photocatalytic degradation rate of the VOCs was calculated as follows:

$$r = \left(\frac{Q}{S} \right) \times \frac{C_{in}}{100} \times R(\%) \quad (1)$$

$$RE (\%) = \frac{C_{in} - C_{out}}{C_{in}} \times 100 \quad (2)$$

where RE is the VOCs' removal efficiency, C_{in} and C_{out} are the inlet and outlet VOCs' concentration ($\text{mM} \cdot \text{m}^{-3}$), respectively, Q is the volumetric flow rate ($\text{m}^3 \cdot \text{h}^{-1}$), and S is the medium surface (m^2).

The Langmuir–Hinshelwood (L-H) model generally represents the degradation kinetics. This model is defined by the following equation [27–29]:

$$r_o = \frac{k \cdot K \cdot C_0}{1 + KC_0} \text{ or } \frac{1}{r_o} = \frac{1}{kK} \cdot \frac{1}{C_0} + \frac{1}{k} \quad (3)$$

where r_0 is the initial reaction rate ($\text{mM}\cdot\text{m}^{-3}\cdot\text{s}^{-1}$), k is the reaction rate constant ($\text{mM}\cdot\text{m}^{-3}\cdot\text{s}^{-1}$), and K is the adsorption constant ($\text{m}^3\cdot\text{mM}^{-1}$).

The slope of the curve $C = f(\text{time})$, where the influence of the by-products is assumed to be negligible, determines the initial reaction rate. The values of the L-H constants are determined from the slope and intercept of the plot $r_0^{-1} = f(C_0^{-1})$.

Assuming that the mass transfer is not the limiting step, and that the effect of the intermediate products is negligible, then the reaction rate can be expressed according to Equation (3) [29]. In this model, the adsorption and desorption reactions are neglected in comparison to the oxidation mechanism. A continuous plug flow reactor at a steady state is considered. The distribution of the pollutants along the axial direction should not be ignored. The continuity equation for a pollutant is denoted as follows:

$$u \cdot \frac{dC}{dz} = -r \quad (4)$$

In this equation, z is the axial position in the reactor. After integration, the previous equation becomes

$$\frac{\ln(C_{in}/C_{out})}{C_{in} - C_{out}} = \frac{k_{app} \cdot K \cdot L}{u} \frac{1}{C_{in} - C_{out}} - K \quad (5)$$

where L is the reactor length (m), u is the superficial gas velocity ($\text{m}\cdot\text{s}^{-1}$), and C_{in} and C_{out} are the inlet and outlet concentrations. The L-H constants k_{app} and K are obtained by fitting the results of each concentration and flow rate with the linear equation. The cross-correlation coefficient is obtained by the covariance of k_{app} and K divided by the norm deviation of each modulus k_{app} and K .

The overall mass balances of the contaminant on the gaseous and solid phases in a continuous reactor result in the following relations [30,31].

In the gas phase:

$$u \cdot \frac{dC}{dz} + k_m \cdot a_v \cdot (C - C_s) = 0 \quad (6)$$

In the solid phase:

$$k_m \cdot a_v \cdot (C - C_s) = \frac{k_{app} \cdot K \cdot C_s}{1 + K \cdot C_s} \quad (7)$$

where C and C_s are the concentrations in the gas phase of the overall and average surface of the VOCs ($\text{mM}\cdot\text{m}^{-3}$), respectively, k_m is the mass transfer coefficient ($\text{m}\cdot\text{s}^{-1}$), and a_v is the average area per unit volume of the reactor ($\text{m}^2\cdot\text{m}^{-3}$).

Assuming a linear transfer gradient, the material flux J_f through the film is written according to the Fick law, integrated over the thickness δ of the film [32].

$$J_f = \frac{D}{\delta} \cdot (C_b - C_s) = k_f \cdot (C_b - C_s) \quad (8)$$

where δ is the thickness of the external film, C_b is the core concentration of the fluid, C_s is the concentration on the surface of the adsorbent grain, k_f is the external mass transfer coefficient, and D is the diffusion coefficient.

The film thickness δ varies with the operating conditions, such as the turbulence, grain size, and fluid viscosity. Several semi-empirical correlations were established to obtain the external mass transfer coefficient k_f . The dimensionless numbers of Reynolds (Re), Schmidt (Sc), and Sherwood (Sh) translate these parameters.

$$Re = \frac{2 \cdot R_p \cdot \rho \cdot U_0}{\mu} \quad Sc = \frac{\mu}{\rho \cdot D_{mol}} \quad Sh = \frac{d_{eq} \cdot k_f}{D_{mol}} \quad (9)$$

where d_{eq} is the equivalent diameter, ρ is the fluid density, U_0 is the surface velocity, μ is the fluid dynamic viscosity, and D_{mol} is the molecular diffusion coefficient of the solute in the fluid.

$$D_{mol} = \frac{10^{-3} \cdot \sqrt{\frac{29+M}{29 \cdot M}} \cdot T^{1.75}}{(20.1^{\frac{1}{3}} + V_m^{\frac{1}{3}})^2 \cdot P_{atm}} \quad (10)$$

where P is the gas flow pressure (Pa), T is the absolute temperature ($^{\circ}\text{K}$), V_m is the molecular volume of the gas ($\text{m}^3 \cdot \text{m}^{-1}$), and M is the molecular mass of the pollutant ($\text{g} \cdot \text{m}^{-1}$).

2.1. Photocatalytic Reactor Configuration

The catalytic material was a coated fiberglass mat of 20 g/m^2 of colloidal silica which ensured the fixation of 20 g/m^2 of PC500 Millenium titanium dioxide nanoparticles. The PC500 TiO_2 nanoparticles had a diameter of 5 to 10 nm and were in a pure anatase form with an indirect bandgap energy of 3.3 eV. The specific surface area of the TiO_2 nanoparticles was $300 \text{ m}^2/\text{g}$. The coating process consisted of impregnating the fibers using an industrial-sized press. The material preparation was carried out by Ahlstrom Research and Services (Ahlstrom Patent). The plot of the N_2 isotherm showed an adsorption of the fundamental type on a non-porous solid.

The light source was an 80 W UVA lamp (Philips CLEO performance). Its emission spectrum varied from 300 to 400 nm. The pollutant circulated continuously in a tangential flow in the reactor. The reactor was cleaned with an air stream ($2 \text{ m}^3 \cdot \text{h}^{-1}$) under UV light at about $20 \text{ W} \cdot \text{m}^{-2}$ for one hour to avoid possible contamination before starting the experiments. The injection of VOCs was made continuously in the liquid state from a syringe pump system (Kd Scientific Model 100, Holliston, MA, USA). This system was introduced into the circuit as a gas flow.

The flow rate and VOCs' concentrations varied from 1 to $9 \text{ m}^3 \cdot \text{h}^{-1}$ and 30 to $216 \text{ mg} \cdot \text{m}^{-3}$, respectively. A heating tape was wound around the channel at the level of the injection zone to ensure the good evaporation of the pollutants. Valves and a flowmeter (Bronkhorst In-Flow, Grez-sur-Loing, France) were introduced at the reactor inlet to maintain the airflow (Figures 1 and 2). A specific testo sensor monitored the air quality (humidity and temperature). In this study, the values (5%, 30%, 55%, and 80%) for the relative humidity were determined by introducing a column humidifier into the degradation system to provide dry and humid air.

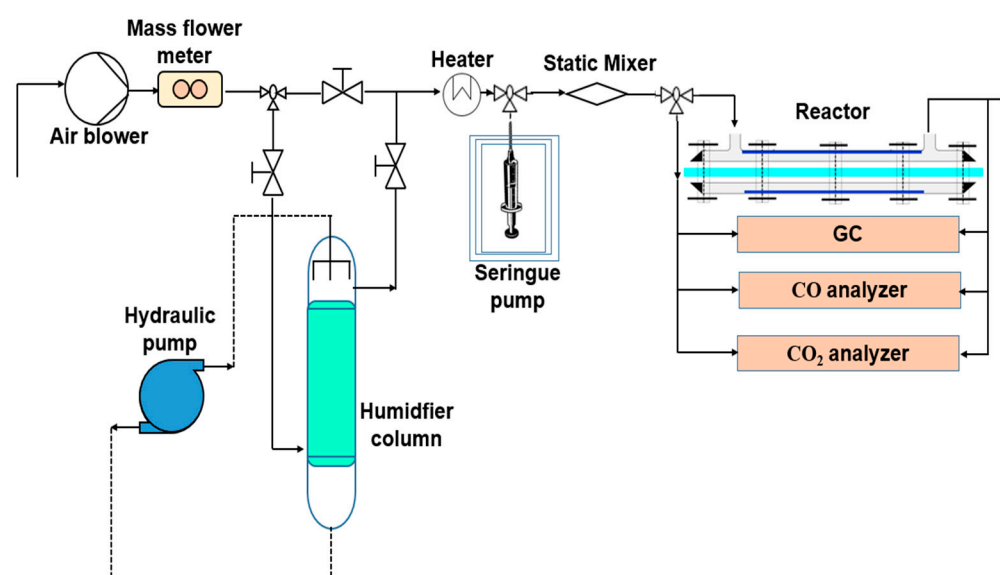


Figure 1. The schematic of the experimental setup.

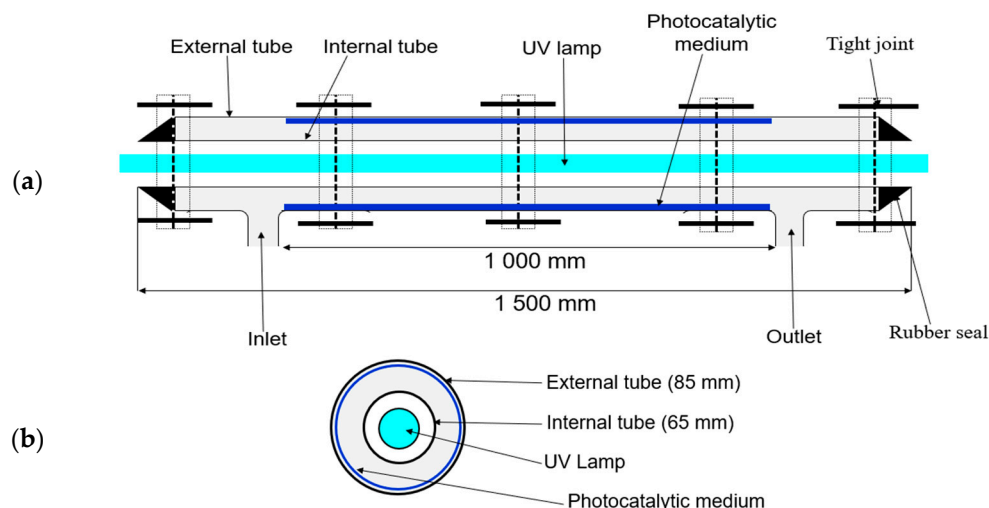


Figure 2. (a) The schematic of the reactor setup and (b) a cross section of the concentric cylindrical Pyrex glass tube reactor.

2.2. Gas Phase Analysis

The VOCs' concentration, before and after the mineralization experiments, was quantified using a gas chromatography (Focus GC) using a flame ionization detector (FID) and an FFAP column (length = 25 m and internal diameter = 0.32 mm). The flow rate of the carrier gas was $1 \text{ mL} \cdot \text{min}^{-1}$. The injector and detector temperatures of the CN were $260 \text{ }^\circ\text{C}$ and $270 \text{ }^\circ\text{C}$, respectively, and $250 \text{ }^\circ\text{C}$ for the CB. The samples were collected in the reactor downstream using a $500 \text{ }\mu\text{L}$ gas-tight syringe and were manually injected into the GC. The CO_2 concentration was quantified using a multi-gas infrared analyzer equipped with GFC (Gas Filter Correlation) technology (MIR 9000 Environment, Verano Brianza, Italy). A TESTO sensor was used to monitor the system's temperature and relative humidity (RH).

3. Results and Discussion

3.1. Effect of Flow Rate and Inlet Concentration

In this section, only the surface step reaction is considered, i.e., the mass transfer is neglected, in order to describe the photocatalytic reaction in the gas–solid phase.

Table 1 presents the semi-empirical formulas necessary to find the external mass transfer coefficient for tangential flow reactors.

Table 1. The semi-empirical formulas for the estimation of k_f .

Reactors	Formulas	Conditions
Tangential flow reactor	$Sh = 1.029 \cdot Re^{0.55} \times Sc^{0.33} \cdot \left(\frac{L}{d_{eq}}\right)^{-0.472}$	Si $Re \leq 2500$
	$Sh = 0.095 \cdot Re^{0.85} \cdot Sc^{0.33} \cdot \left(\frac{L}{d_{eq}}\right)^{-0.472}$	Si $Re \geq 2500$

L : length; d_{eq} : equivalent diameter of the reactor.

Table 2 illustrates the Reynolds number, diffusivity, and mass transfer coefficients for two components at various volumetric flow rates. The values of the coefficients k_f resulting from these correlations are used to determine an equivalent diffusion. The numerical solution of the following equation can be used to evaluate the parameters k and K :

$$C_{in} - C_{out} = \frac{L \cdot k_m \cdot a_v}{2 \cdot u} \cdot \left[C_{in} + \frac{1}{K} + \frac{k}{k_m \cdot a_v} - \sqrt{\left(-C_{in} + \frac{1}{K} + \frac{k}{k_m \cdot a_v}\right)^2 + \frac{4C_{in}}{K}} \right] \quad (11)$$

Table 2. Reynolds number, diffusivity, and mass transfer coefficients.

Q ($\text{m}^3 \cdot \text{h}^{-1}$)	Re	D_{mol} ($\text{cm}^2 \cdot \text{s}^{-1}$)		K_f ($\times 10^3 \text{ m} \cdot \text{s}^{-1}$)	
		CB	CN	CB	CN
1	213			0.40	0.39
3	639			1.02	1.00
6	1279	0.0494	0.0478	1.85	1.81
9	1919			2.60	2.55

Figure 3a,b shows the modeling of the CB and CN degradation rates during photocatalysis.

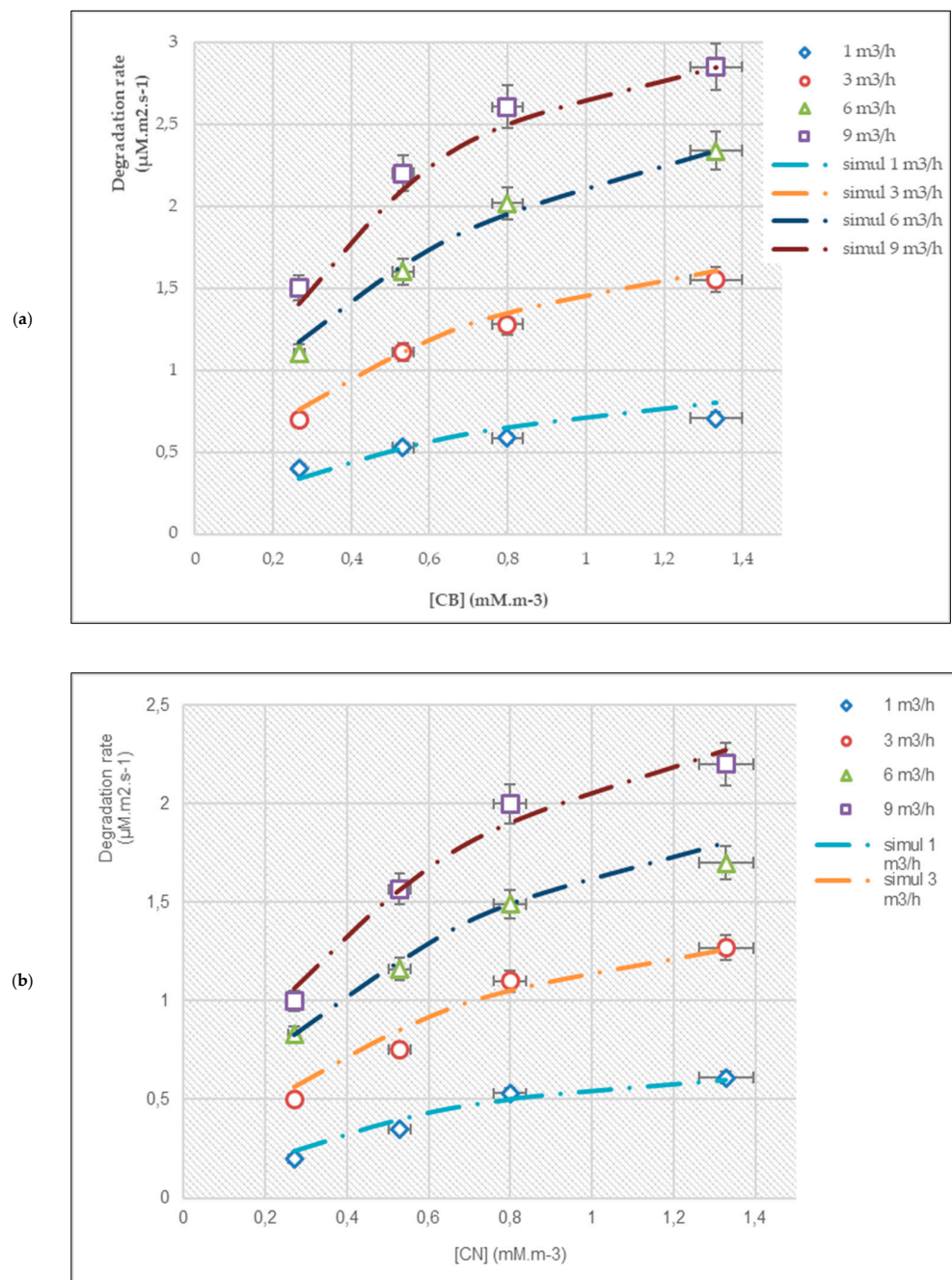


Figure 3. The variation in the degradation rate of CB (a) and CN (b) with the inlet concentration at different flow rates ($I = 20 \text{ W} \cdot \text{m}^{-2}$; $\text{RH} = 30\%$; $T = 20 \text{ }^\circ\text{C}$).

The degradation rates of the two VOCs were identical. Whatever the flow rates, the DR was improved with an increasing concentration. However, CB degraded faster than CN under similar experimental conditions, in terms of the concentration and flow rate. Indeed, for a concentration of $1.328 \text{ mM}\cdot\text{m}^{-3}$, the DR of CB varied from 0.70 to $2.84 \text{ }\mu\text{M}\cdot\text{m}^2\cdot\text{s}^{-1}$ when the flow rate increased from 1 to $9 \text{ m}^3\cdot\text{h}^{-1}$, while the DR of CN varied from 0.60 to $2.20 \text{ }\mu\text{M}\cdot\text{m}^2\cdot\text{s}^{-1}$ for the same flow rate interval. This difference in the DR may be related to the hydrophobicity and stability of the molecules (two aromatic rings) of CN on the surface of TiO_2 . This result is in agreement with a study [33] dealing with six aromatic compounds: benzene, toluene, ethylbenzene, and m-, o-, and p-xylenes. In their investigation, the authors showed that these compounds do not have the same photocatalytic reactivity. Benzene was the most challenging compound to degrade due to its extreme stability and the equivalence of its six carbons.

The simulation results shown in Figure 3a,b based on the L-H model are summarized in Table 3.

Table 3. k and K values for CB and CN for model TM.

VOCs	k ($\text{mM}/\text{m}^3\cdot\text{s}$)	K (m^3/mM)	R ² (%)
CB	0.92	8.4	99
CN	0.10	9.1	99

From Table 3, it is interesting to note that the kinetic constants (k) of the L-H model for CN are very different compared to those for CB. However, the two pollutants' adsorption constants (K) were similar. This trend can be explained by the hydrophobicity and stability of the pollutants.

The degradation rates improved with an increasing flow rate and concentration. Indeed, as the flow rate and concentration increased, the species' movement to the catalyst's interface was enhanced. This analysis is in accordance with the work of Tulebekov and his group [34], who stated that the degradation rate improves with an increasing flow rate and VOC concentration. These results also agree with literature [27–29]. Serhane and his co-workers [35] argued that the increase in the degradation rate is related to the availability of the active species, i.e., if the formation of the first radical species is facilitated; in this case, the degradation of the adsorbed pollutants starts faster, and the residence time could be shorter.

3.2. The Effect of Relative Humidity on the Degradation Rate

To corroborate the results obtained from the experimental tests, the Langmuir–Hinshelwood bimolecular model was used [36]. In this model, the water–VOC system is assimilated into a binary system. The degradation kinetics can be expressed as follows:

$$r_A = k_A \cdot F_A \cdot F_W \quad (12)$$

$$F_A = \frac{K_A \cdot C_A}{(1 + K_A \cdot C_A + K_w \cdot C_w)} \quad (13)$$

$$F_w = \frac{K'_w \cdot C_w}{(1 + K'_A \cdot C_A + K'_w \cdot C_w)} \quad (14)$$

$$r_A = k_A \cdot \frac{K_A \cdot C_A}{(1 + K_A \cdot C_A + K_w \cdot C_w)} \cdot \frac{K'_w \cdot C_w}{(1 + K'_A \cdot C_A + K'_w \cdot C_w)} \quad (15)$$

The constants k_A and K_A are obtained by considering the mass transfer in the previous study, with a relative humidity value of 5% (dry air). C_w is the water vapor concentration, K_w is the Langmuir adsorption constant of the water, and K'_A and K'_w are the competitive adsorption constant of the pollutant and water.

Table 4 displays values for the Langmuir-Hinshelwood model parameters for the Volatile Organic Compounds (VOCs) types, including reaction rate constants and adsorption constants.

Table 4. Values for model L-H.

VOCs	k_A ($\text{mM}\cdot\text{m}^{-3}\cdot\text{s}^{-1}$)	K_A ($\text{m}^3\cdot\text{mM}^{-1}$)	K_W ($\text{m}^3\cdot\text{mmol}^{-1}$)	K'_A ($\text{m}^3\cdot\text{mmol}^{-1}$)	K'_W ($\text{m}^3\cdot\text{mmol}^{-1}$)
CB	0.920	8.400	0.029	1.500	0.456
CN	0.100	9.100	0.02178	1.756	0.200

Relative humidity (RH) modeling confirmed that H_2O molecules greatly influence the kinetics of VOC conversion in the photocatalytic process. The pace of the simulated and experimental speeds was identical. Petit and his group [29] showed that the photocatalytic removal rate of cyclohexane increases with the amount of water vapor. However, above a certain threshold, there is a detrimental effect on the degradation rate. Refs. [30,37–39] have confirmed this assertion.

Figure 4a,b present the influence of water molecules on treating VOCs during heterogeneous photocatalysis.

The DR increased from 5 to 55% RH, while it decreased beyond 55% RH. The experimental and simulated speeds varied based on the flow and concentration conditions. When compared to CN, a higher CB degradation was observed under this study's humidity conditions. It is well known that the influence of humidity on the degradation of VOCs depends on the nature of the pollutant, especially its hydrophilic character and the concentration of the injected VOCs.

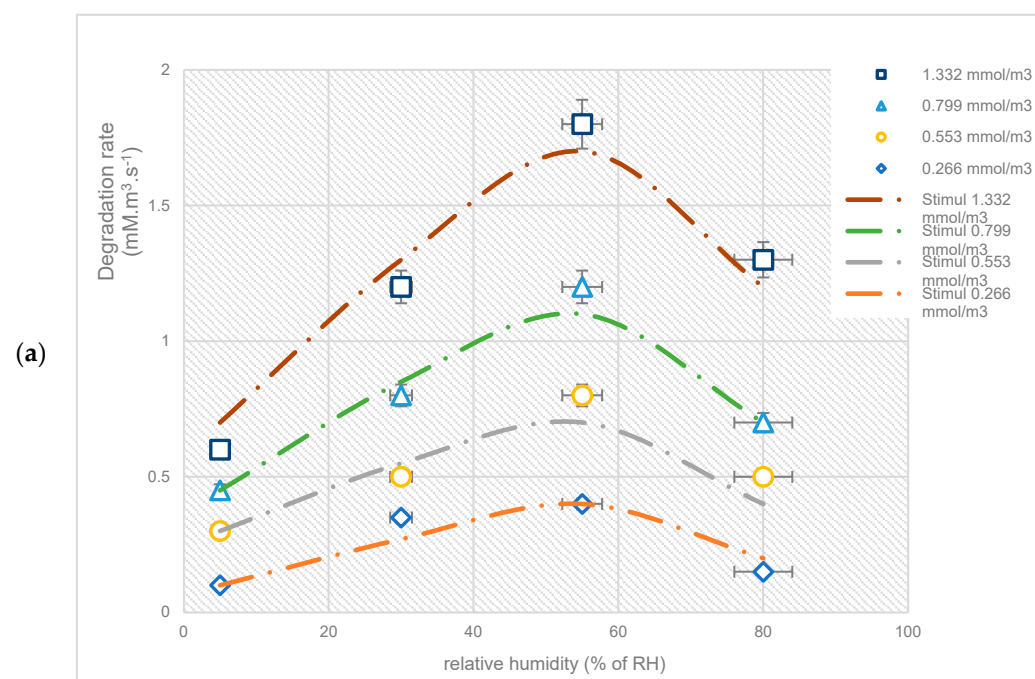


Figure 4. Cont.

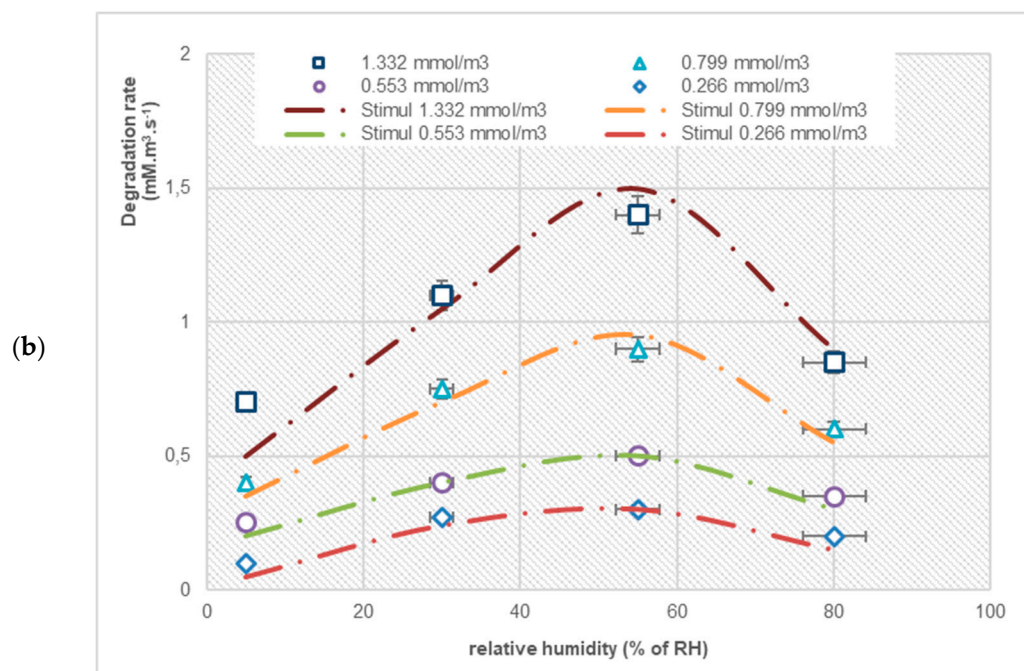
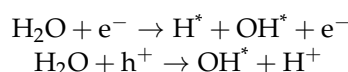
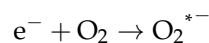


Figure 4. The influence of humidity on the degradation rates of CB (a) and CN (b) ($I = 20 \text{ W}\cdot\text{m}^{-2}$, $T = 20 \text{ }^\circ\text{C}$, $Q = 1 \text{ m}^3\cdot\text{h}^{-1}$).

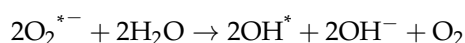
Moreover, TiO_2 has a polar surface, which favors the adoption of water molecules on the catalyst's surface. Even though, there is a small amount of competition with the pollutants on the active's sites, at a low water content, this compaction is accompanied by another photocatalytic reaction (the oxidation of water by photocatalysis), which forms OH° radicals [40]. Therefore, the water molecules in the vapor phase must be consumed over the catalyst surface to promote radical generation. The increase in humidity, thus, facilitates the reactions between the VOC molecules and the radicals formed through the strong OH^* production from H_2O at the interface, as shown in the following reactions:



Oxygen can be transformed into a superoxide anion (O_2^{*-}) by reacting with the photo-generated electrons on the surface of the catalyst, according to the following reaction [15]:



In the presence of water molecules, the superoxide anion (O_2^{*-}) can react with water molecules to generate OH^* :



Thus, increasing the amount of water can lead to an increase in the degradation rate due to the generation of more OH^* radicals.

However, excess water can negatively impact the conversion of pollutants, as water molecules can compete with organic compounds on TiO_2 adsorption sites. Comparing the degradation rate achieved in dry air (RH 5%) and wet air, it was observed that water has a beneficial effect. However, when the humidity level exceeded 55% RH, the adsorption constant significantly decreased, which has been supported by previous studies [28,35,40].

The value of the reaction constant can assume a minimum under dry air conditions and a maximum at about 55% relative humidity, and then decreases with increasing humidity. Under high-humidity conditions, the VOC must first penetrate the layers of

water molecules before interacting with the catalyst surface or any radicals generated in the reactor. The lack of H₂O molecules on the TiO₂ surface limits radical generation in a dry air stream (5%). The water molecule favors photocatalytic reactions under relatively humid conditions (5% to 55%).

At a high humidity (80%), the mole fraction of water submerges the TiO₂ adsorption sites. Mass transfer on and/or into the water film on the TiO₂ surface dominates any potential photocatalytic reaction, as demonstrated by [41]. Therefore, the DR of the VOCs decreases regardless of the concentration of the VOCs in the medium.

The work of [42] on treating trichloromethane by photocatalysis showed that photocatalytic degradation is generally affected by H₂O molecules. In most cases, the complete absence of water vapor is fatal to photocatalysis because it directly affects the amount of OH* formed. In addition, a very high relative humidity value can negatively affect the process due to competition between the water and pollutants. Zang and his co-workers [43] made the same remark in their study of the effect of relative humidity on the photocatalytic degradation mechanism of gaseous styrene.

3.3. Selectivity of CO₂

Photocatalysis allows for the transformation of many VOCs into CO₂ and H₂O. The classic reaction of this chemical mechanism can be summarized as follows:



The selectivity is determined by the following formula [44]:

$$\text{CO}_x \text{selectivity} = \frac{[\text{CO}_x]_{\text{in}} - [\text{CO}_x]_{\text{out}}}{\text{Nc} \cdot \text{RE}(\%) \cdot [\text{VOC}]_{\text{in}}} \cdot 10^4 \quad (16)$$

where Nc is the number of carbon atoms in the pollutant, RE(%) is the removal efficiency, x = 1 for CO and x = 2 for CO₂, and [CO_x]_{in} and [CO_x]_{out} are, respectively, the concentrations in ppm of CO_x at the inlet and outlet of the reactor, and [VOC]_{in} is the inlet concentration of the VOC in ppm.

3.3.1. The CO_x Selectivity with a Variation in the Flow Rate and VOC Concentration

Figures 5 and 6 display the selectivity of the VOCs, showing similar variations in the CO₂ selectivity of CB and CN. The CO₂ selectivity decreased with an increasing flow rate and concentration. The CO₂ selectivity of CB varied from 49% to 15% for a concentration of 90 mg·m⁻³, when the flow rate was increased from 1 to 9 m³/h. For a flow rate of 3 m³/h, the CO₂ selectivity of CB varied from 59% to 30%, when the concentration was increased from 30 to 150 mg·m⁻³.

For CN, the CO₂ selectivity varied from 60% to 21% for a concentration of 130 mg·m⁻³ when the flow rate increased from 1 to 9 m³/h. For a flow rate of 3 m³/h, the CO₂ selectivity of CB varied from 65% to 40% when the concentration increased from 44 to 216 mg·m⁻³.

Indeed, during the photocatalytic mechanism, the number of reactive species photo-generated and the active sites of the support remained constant. Thus, a small fraction was mineralized into CO₂ for high concentrations of pollutants.

The improvement in CO₂ selectivity was noticeable for small concentrations of pollutants injected at the inlet of the reactor, because the availability of the active sites of the catalyst remained greater, so the compounds were easily converted into CO₂. Several studies [19,43–45], are unanimous regarding the fact that increasing the initial concentration and flow rate decreases the CO₂ selectivity during the photocatalytic process.

The products of photocatalytic degradation are generally CO₂ and H₂O. However, the identification of CO at the reactor outlet has often been reported [45]. This point was found in this study only regarding the photocatalytic degradation of CN. Accordingly, the following figure shows the small amount of CO released.

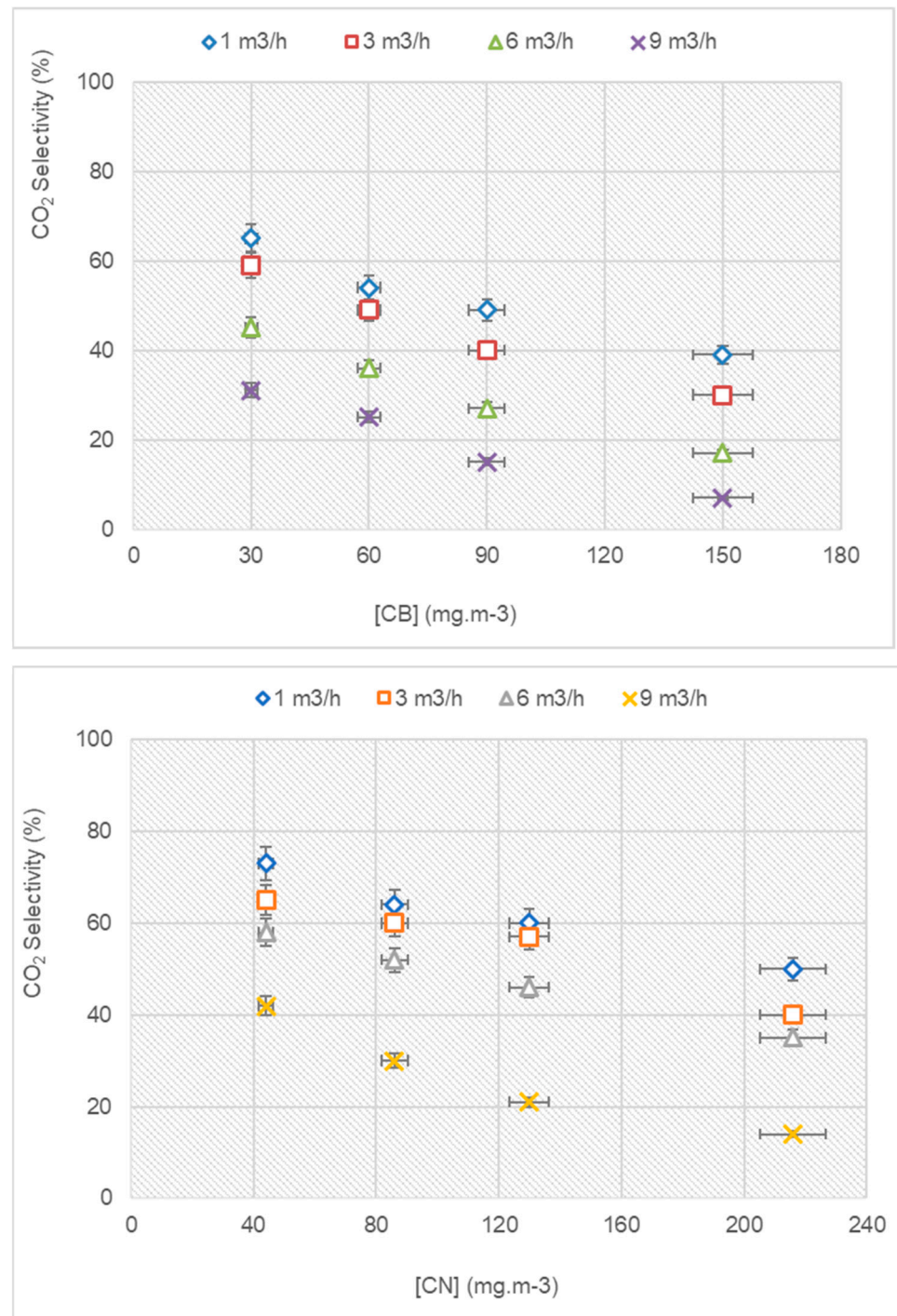


Figure 5. The variation in the CO₂ selectivity of CB and CN at different flow rates and inlet concentrations ($I = 20 \text{ W}\cdot\text{m}^{-2}$; $\text{RH} = 30\%$; $T = 20 \text{ }^\circ\text{C}$).

3.3.2. CO_x Selectivity with Variation in Humidity

The evaluation of CO₂ selectivity in the presence of humid air was performed to determine the impact of the RH on CO₂ production. As observed (Figure 7), the variations in CO₂ selectivity were similar for both VOCs. Regarding CB, the CO₂ selectivity showed a peak at 55% RH, regardless of the VOC concentration. Similarly, regarding CN, the CO₂ selectivity also showed a peak at 55% RH. The CO₂ selectivity of CB increased from 35% to 54%, and then decreased to 36%, at a concentration of 19 ppm. For the same concentration, the CO₂ selectivity of CN increased from 50% to 66%, and then decreased to 52%. This same remark was made by [45].

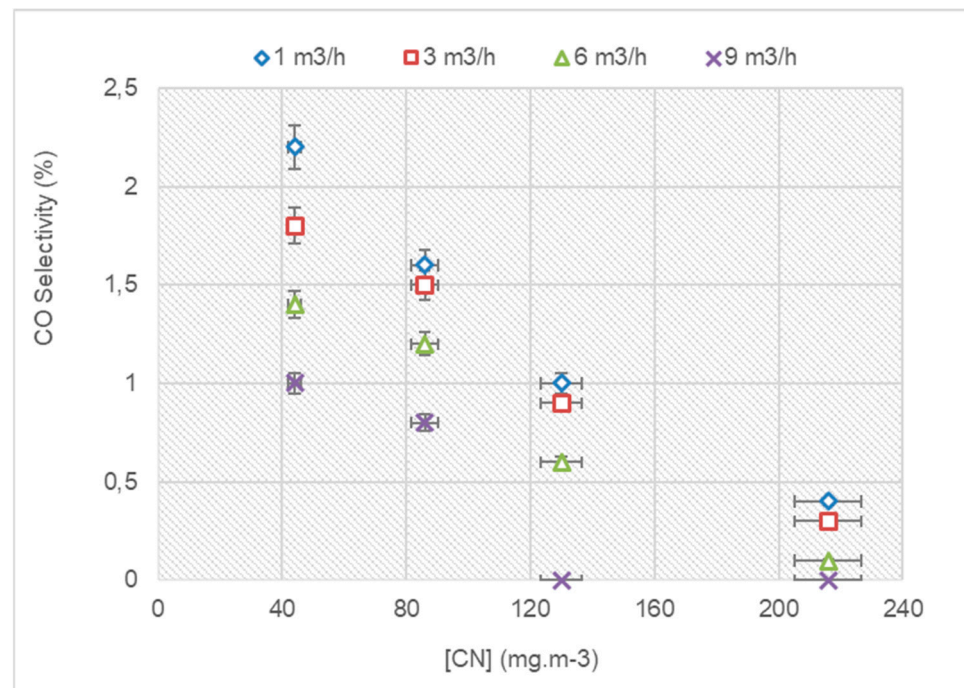


Figure 6. The variation in the CO selectivity of CN at different flow rates and inlet concentrations (RH = 30%; T = 0 °C).

This study shows that, above a specific value, the humidity harms the mineralization of VOCs, leading to a decrease in CO selectivity (Figure 8). This result seems logical because, at a crucial RH, an adsorption competition between water molecules and organic compounds takes place on the surface of TiO₂ leading to a decrease in mineralization. The same conclusion was reached by Chikh and her group [45] following a study of the photocatalytic degradation of VOCs.

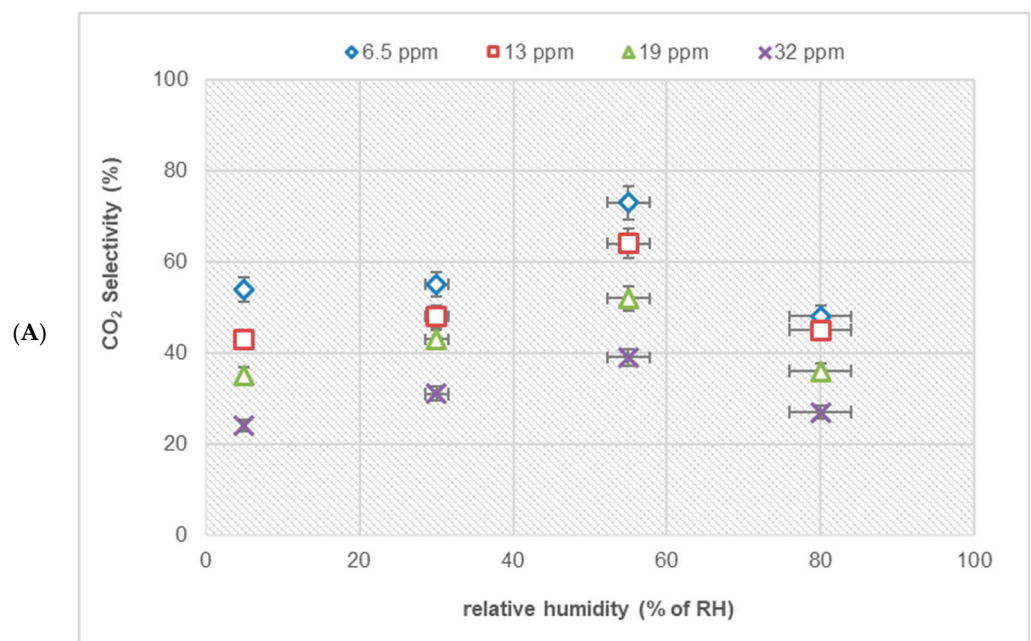


Figure 7. Cont.

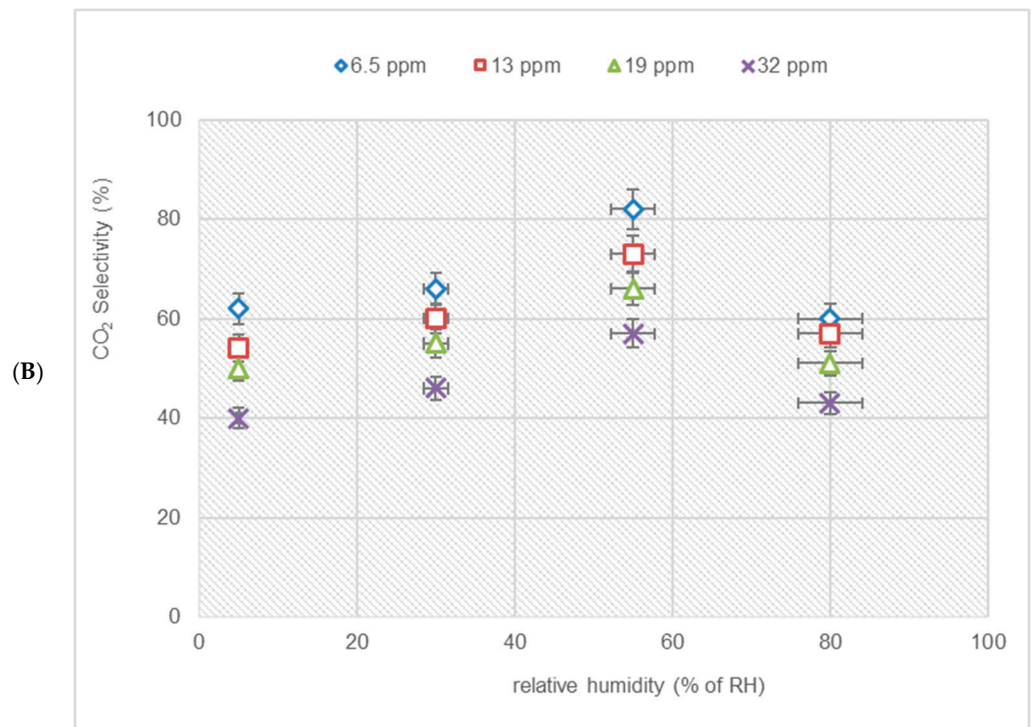


Figure 7. The variation in the CO₂ selectivity (%) of CB (A) and CN (B) at different humidity and inlet concentrations ($I = 20 \text{ W}\cdot\text{m}^{-2}$; $Q = 1 \text{ m}^3\cdot\text{h}^{-1}$; $T = 20 \text{ }^\circ\text{C}$).

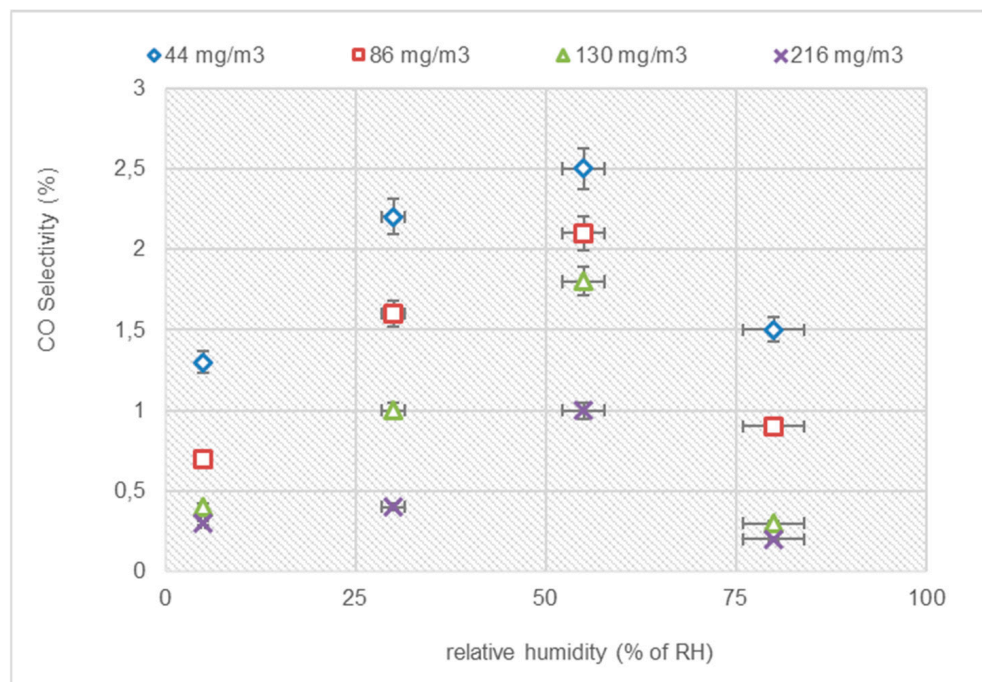


Figure 8. The variation in the CO selectivity (%) of CN at different humidity and inlet concentrations ($I = 20 \text{ W}\cdot\text{m}^{-2}$; $Q = 1 \text{ m}^3\cdot\text{h}^{-1}$; $T = 20 \text{ }^\circ\text{C}$).

Table 5 compares reaction rate constants (k) and adsorption constants (K) for various pollutants processed in different types of reactors, as reported in the literature and this study.

Table 5. A comparison of k and K values obtained from the literature.

References	Reactors	Pollutants	k ($\text{mM}\cdot\text{m}^{-3}\cdot\text{s}^{-1}$)	K ($\text{m}^3\cdot\text{mM}^{-1}$)
[29]	Front-flow continuous reactor	Cyclohexane	0.025	7.12
[28]	Annular reactor	Isovaleraldehyde	0.49	1.62
		Trimethylamine	0.69	1.19
[27]	Continuous reactor	Chloroform	0.04	2.74
		Glutaraldehyde	0.09	1.16
This study	Cylindric reactor	Chlorobenzene	0.92	8.4
		Chloronaphthalene	0.10	9.1

The photocatalytic results are better than those found in the literature. This difference is due to the reactor configuration. The present configuration has a small air thickness, enhancing the mass transfer and obtaining attractive k and K values. In addition, it is interesting to note that these constants are not flow rate dependent. The influence of the flow regime is integrated completely through the parameter km . In fact, the separation of the mass transfer and the chemical reaction steps is obtained.

4. Conclusions

Based on this study's findings, applying the L-H model for treating air containing chlorobenzene and chloronaphthalene using TiO_2 photocatalysis demonstrates promising results. The degradation rates (DRs) were notably influenced by the inlet concentrations of the VOCs and the air effluent flow rate. Higher concentrations of VOCs and increased airflow rates correlated with improved DRs, suggesting an enhanced mass transfer and availability of active species. The facilitation of the initial radical species formation was identified as a critical factor in accelerating the degradation of the adsorbed pollutants, thereby reducing the residence time.

Furthermore, the L-H model reveals the significant impact of water molecules on the kinetics of VOC conversion during the photocatalytic process. An increase in water content from 5% to 55% enhanced the degradation rate due to the more significant generation of OH^* radicals. However, a counteractive effect was observed with higher water quantities, wherein competition for the TiO_2 adsorption sites reduced pollutant conversion. Interestingly, this study highlights a consistently higher chlorobenzene than chloronaphthalene degradation rate across varying flow rates, concentrations, and relative humidity conditions. These findings contribute valuable insights into optimizing photocatalytic processes for treating specific volatile organic compounds.

Author Contributions: Investigation, N.A.K., N.B. and Y.S.; formal analysis, N.A.K., N.B. and Y.S.; visualization, N.A.K., N.B. and Y.S.; writing original review, N.A.K., N.B. and Y.S.; conceptualization, L.K., S.L.C. and W.E.; funding acquisition L.K., S.L.C. and W.E.; methodology, L.C., A.B., A.A. and A.A.A.; project administration, L.C., A.B., A.A. and A.A.A.; supervision, L.C., A.B., A.A. and A.A.A.; writing-review and editing, L.C., A.B., A.A. and A.A.A. All authors have read and agreed to the published version of the manuscript.

Funding: This research received no external funding.

Institutional Review Board Statement: Not Applicable.

Informed Consent Statement: Not Applicable.

Data Availability Statement: The data supporting the conclusions of this study are accessible from the corresponding author upon reasonable request. The data are not publicly available due to privacy.

Acknowledgments: The authors gratefully acknowledge the support and funding provided by the Deanship of Scientific Research at Imam Mohammad Ibn Saud Islamic University (IMSIU) through the Research Partnership grant, grant number IMSIU-RP23076.

Conflicts of Interest: The authors declare no conflicts of interest.

References

1. Abidi, M.; Hajjaji, A.; Bouzaza, A.; Lamaa, L.; Peruchon, L.; Brochier, C.; Rtimi, S.; Wolbert, D.; Bessais, B.; Assadi, A.A. Modeling of indoor air treatment using an innovative photocatalytic luminous textile: Reactor compactness and mass transfer enhancement. *Chem. Eng. J.* **2022**, *430*, 132636. [[CrossRef](#)]
2. Abiev, R.S.; Sladkovskiy, D.A.; Semikin, K.V.; Murzin, D.Y.; Rebrov, E.V. Non-thermal plasma for process and energy intensification in dry reforming of methane. *Catalysts* **2020**, *10*, 1358. [[CrossRef](#)]
3. Ahmadi, Y.; Kim, K.H. Modification strategies for visible-light photocatalysts and their performance-enhancing effects on photocatalytic degradation of volatile organic compounds. *Renew. Sustain. Energy Rev.* **2024**, *189*, 113948. [[CrossRef](#)]
4. Alcázar-Medina, T.L.; Chairez-Hernández, I.; Lemus-Santana, A.A.; Núñez-Núñez, C.M.; Proal-Nájera, J.B. Amoxicillin Degradation by TiO₂ P25 Solar Heterogeneous Photocatalysis: Influence of pH and Oxidizing Agent H₂O₂ Addition. *Appl. Sci.* **2023**, *13*, 7857. [[CrossRef](#)]
5. Assadi, A.A. Efficient Photocatalytic Luminous Textile for Simulated Real Water Purification: Advancing Economical and Compact Reactors. *Materials* **2024**, *17*, 296. [[CrossRef](#)]
6. Ashley, N.A.; McBride, N.; Krumholt, J.; Baker, B.; Valsaraj, K.T. Photocatalytic Reaction of Gas-Phase Naphthalene on Paint- and Sunscreen-Coated Surfaces. *ISRN Chem. Eng.* **2012**, *2012*, 72479. [[CrossRef](#)]
7. Assadi, A.A.; Bouzaza, A.; Wolbert, D. Photocatalytic oxidation of trimethylamine and isovaleraldehyde in an annular reactor: Influence of the mass transfer and the relative humidity. *J. Photochem. Photobiol. A Chem.* **2012**, *236*, 61–69. [[CrossRef](#)]
8. Bai, S.; Qiu, H.; Song, M.; He, G.; Wang, F.; Liu, Y.; Guo, L. Porous fixed-bed photoreactor for boosting C–C coupling in photocatalytic CO₂ reduction. *eScience* **2022**, *2*, 428–437. [[CrossRef](#)]
9. Boulamanti, A.K.; Korologos, C.A.; Philippopoulos, C.J. The rate of photocatalytic oxidation of aromatic volatile organic compounds in the gas-phase. *Atmos. Environ.* **2008**, *42*, 7844–7850. [[CrossRef](#)]
10. Chang, Z.; Wang, C.; Zhang, G. Progress in degradation of volatile organic compounds based on low-temperature plasma technology. *Plasma Process. Polym.* **2020**, *17*, 1900131. [[CrossRef](#)]
11. Chen, J.; Zhang, L.; Zhu, W.; Li, G.; An, T. Atomic-level insight into effect of substrate concentration and relative humidity on photocatalytic degradation mechanism of gaseous styrene. *Chemosphere* **2022**, *291*, 133074. [[CrossRef](#)]
12. Cui, Y.; Ding, Z.; Sun, Y.; Yi, Y.; Xu, F.; Zhang, Q.; Wang, W. A theoretical study of OH radical-initiated atmospheric oxidation of 1-chloronaphthalene. *Chem. Phys. Lett.* **2018**, *699*, 40–47. [[CrossRef](#)]
13. Dahiru, U.H.; Saleem, F.; Zhang, K.; Harvey, A. Plasma-assisted removal of methanol in N₂, dry and humidified air using a dielectric barrier discharge (DBD) reactor. *RSC Adv.* **2022**, *12*, 10997–11007. [[CrossRef](#)]
14. Ebrahimi, H.; Shahna, F.G.; Bahrami, A.; Jaleh, B.; Abedi, K.A.D. Photocatalytic degradation of volatile chlorinated organic compounds with ozone addition. *Arch. Environ. Prot.* **2017**, *43*, 65–72. [[CrossRef](#)]
15. Khezami, L.; Assadi, A.A. Treatment of Mixture Pollutants with Combined Plasma Photocatalysis in Continuous Tubular Reactors with Atmospheric-Pressure Environment: Understanding Synergetic Effect Sources. *Materials* **2023**, *16*, 6857. [[CrossRef](#)]
16. He, S.; Chen, Y.; Li, X.; Zeng, L.; Zhu, M. Heterogeneous Photocatalytic Activation of Persulfate for the Removal of Organic Contaminants in Water: A Critical Review. *ACS ES&T Eng.* **2022**, *2*, 527–546. [[CrossRef](#)]
17. Jaison, A.; Mohan, A.; Lee, Y.C. Recent Developments in Photocatalytic Nanotechnology for Purifying Air Polluted with Volatile Organic Compounds: Effect of Operating Parameters and Catalyst Deactivation. *Catalysts* **2023**, *13*, 407. [[CrossRef](#)]
18. Qi, J.; Wang, C.; Sun, J.; Li, S. TiO₂ Assisted Photocatalytic Decomposition of 2-Chloronaphthalene on Iron Nanoparticles in Aqueous Systems: Synergistic Effect and Intermediate Products. *Russ. J. Phys. Chem. A* **2019**, *93*, 1620–1626. [[CrossRef](#)]
19. Jo, W.K.; Park, K.H. Heterogeneous photocatalysis of aromatic and chlorinated volatile organic compounds (VOCs) for non-occupational indoor air application. *Chemosphere* **2004**, *57*, 555–565. [[CrossRef](#)] [[PubMed](#)]
20. Kim, S.B.; Hong, S.C. Kinetic study for photocatalytic degradation of volatile organic compounds in air using thin film TiO₂ photocatalyst. *Appl. Catal. B Environ.* **2002**, *35*, 305–315. [[CrossRef](#)]
21. Kenfoud, H.; Baaloudj, O.; Nasrallah, N. Structural and electrochemical characterizations of Bi₁₂CoO₂₀ sillenite crystals: Degradation and reduction of organic and inorganic pollutants. *J. Mater. Sci. Mater. Electron.* **2021**, *32*, 16411–16420. [[CrossRef](#)]
22. Koné, N.Z.A.; Belkessa, N.; Serhane, Y.; Coulibaly, S.L.; Kamagate, M. Chlorobenzene Mineralization Using Plasma/Photocatalysis Hybrid Reactor: Exploiting the Synergistic Effect. *Catalysts* **2023**, *13*, 431. [[CrossRef](#)]
23. Kong, C.P.Y.; Suhaimi, N.A.A.; Shahri, N.N.M.; Lim, J.W.; Nur, M.; Hobley, J.; Usman, A. Auramine O UV Photocatalytic Degradation on TiO₂ Nanoparticles in a Heterogeneous Aqueous Solution. *Catalysts* **2022**, *12*, 975. [[CrossRef](#)]
24. Li, J.; Xie, X.; Li, L.; Wang, X.; Wang, H.; Jing, S.; Ying, Q.; Qin, M.; Hu, J. Fate of Oxygenated Volatile Organic Compounds in the Yangtze River Delta Region: Source Contributions and Impacts on the Atmospheric Oxidation Capacity. *Environ. Sci. Technol.* **2022**, *56*, 11212–11224. [[CrossRef](#)] [[PubMed](#)]

25. Drhimer, F.; Rahmani, M.; Regraguy, B.; El Hajjaji, S.; Mabrouki, J.; Amrane, A.; Fourcade, F.; Assadi, A.A. Treatment of a Food Industry Dye, Brilliant Blue, at Low Concentration Using a New Photocatalytic Configuration. *Sustainability* **2023**, *15*, 5788. [[CrossRef](#)]
26. Masresha, G.; Jabasingh, S.A.; Kebede, S.; Doo-Arhin, D.; Assefa, M. A review of prospects and challenges of photocatalytic decomposition of volatile organic compounds (VOCs) under humid environment. *Can. J. Chem. Eng.* **2023**, *101*, 6905–6918. [[CrossRef](#)]
27. Maung, T.Z.; Bishop, J.E.; Holt, E.; Turner, A.M.; Pfrang, C. Indoor Air Pollution and the Health of Vulnerable Groups: A Systematic Review Focused on Particulate Matter (PM), Volatile Organic Compounds (VOCs) and Their Effects on Children and People with Pre-Existing Lung Disease. *Int. J. Environ. Res. Public Health* **2022**, *19*, 8752. [[CrossRef](#)]
28. Mohammed, S.S.; Shnain, Z.Y.; Abid, M.F. Use of TiO₂ in Photocatalysis for Air Purification and Wastewater Treatment: A Review. *Eng. Technol. J.* **2022**, *3*, 1131–1143. [[CrossRef](#)]
29. Petit, N.; Bouzaza, A.; Wolbert, D.; Petit, P.; Dussaud, J. Photocatalytic degradation of gaseous perchloroethylene in continuous flow reactors: Rate enhancement by chlorine radicals. *Catal. Today* **2007**, *124*, 266–272. [[CrossRef](#)]
30. Assadi, A.A.; Baaloudj, O.; Khezami, L.; Ben Hamadi, N.; Mouni, L.; Assadi, A.A.; Ghorbal, A. An Overview of Recent Developments in Improving the Photocatalytic Activity of TiO₂-Based Materials for the Treatment of Indoor Air and Bacterial Inactivation. *Materials* **2023**, *16*, 2246. [[CrossRef](#)]
31. Rissanen, K.; Aalto, J.; Gessler, A.; Hölttä, T.; Rigling, A.; Schaub, M.; Bäck, J. Drought effects on volatile organic compound emissions from Scots pine stems. *Plant. Cell Environ.* **2022**, *45*, 23–40. [[CrossRef](#)] [[PubMed](#)]
32. Rouf, Z.; Dar, I.Y.; Javaid, M.; Dar, M.Y.; Jehangir, A. Volatile Organic Compounds Emission from Building Sector and Its Adverse Effects on Human Health. In *Ecological and Health Effects of Building Materials*; Springer International Publishing: Berlin/Heidelberg, Germany, 2022; pp. 67–86. [[CrossRef](#)]
33. Serhane, Y.; Belkessa, N.; Bouzaza, A.; Wolbert, D.; Assadi, A.A. Continuous air purification by front flow photocatalytic reactor: Modelling of the influence of mass transfer step under simulated real conditions. *Chemosphere* **2022**, *295*, 133809. [[CrossRef](#)]
34. Tulebekov, Y.; Orazov, Z.; Satybaldiyev, B.; Snow, D.D.; Schneider, R.; Uralbekov, B. Reaction Steps in Heterogeneous Photocatalytic Oxidation of Toluene in Gas Phase—A Review. *Molecules* **2023**, *28*, 6451. [[CrossRef](#)]
35. Wang, Y.; Ding, L.; Shi, Q.; Liu, S.; Qian, L.; Yu, Z.; Wang, H.; Lei, J.; Gao, Z.; Long, H.; et al. Volatile organic compounds (VOC) emissions control in iron ore sintering process: Recent progress and future development. *Chem. Eng. J.* **2022**, *448*, 137601. [[CrossRef](#)]
36. Wu, J.; Chen, Y.; Chien, Y.; Kurioka, T.; Sone, M.; Chen, C.; Chang, T.M.; Hsu, Y. Photocatalytic Fibers for Environmental Purification: Challenges and Opportunities in the Post-Pandemic Era. *Adv. Energy Sustain. Res.* **2023**, *5*, 2300212. [[CrossRef](#)]
37. Xu, P.; Ding, C.; Li, Z.; Yu, R.; Cui, H.; Gao, S. Photocatalytic degradation of air pollutant by modified nano titanium oxide (TiO₂) in a fluidized bed photoreactor: Optimizing and kinetic modeling. *Chemosphere* **2023**, *319*, 137995. [[CrossRef](#)] [[PubMed](#)]
38. Yamazaki, S.; Tsukamoto, H.; Araki, K.; Tanimura, T.; Tejedor-Tejedor, I.; Anderson, M.A. Photocatalytic degradation of gaseous tetrachloroethylene on porous TiO₂ pellets. *Appl. Catal. B Environ.* **2001**, *33*, 109–117. [[CrossRef](#)]
39. Zadi, T.; Assadi, A.A.; Nasrallah, N.; Bouallouche, R.; Tri, P.N.; Bouzaza, A.; Azizi, M.M.; Maachi, R.; Wolbert, D. Treatment of hospital indoor air by a hybrid system of combined plasma with photocatalysis: Case of trichloromethane. *Chem. Eng. J.* **2018**, *349*, 276–286. [[CrossRef](#)]
40. Zatta, D.; Segata, M.; Biasioli, F.; Allegretti, O.; Bochicchio, G.; Verucchi, R.; Chiavarini, F.; Cappellin, L. Comparative Analysis of Volatile Organic Compound Purification Techniques in Complex Cooking Emissions: Adsorption, Photocatalysis and Combined Systems. *Molecules* **2023**, *28*, 7658. [[CrossRef](#)]
41. Zhang, L.; Moralejo, C.; Anderson, W.A. A review of the influence of humidity on photocatalytic decomposition of gaseous pollutants on TiO₂-based catalysts. *Can. J. Chem. Eng.* **2020**, *98*, 263–273. [[CrossRef](#)]
42. Zhang, L.; Sawell, S.; Moralejo, C.; Anderson, W.A. Heterogeneous photocatalytic decomposition of gas-phase chlorobenzene. *Appl. Catal. B Environ.* **2007**, *71*, 135–142. [[CrossRef](#)]
43. Zhang, M.; An, T.; Fu, J.; Sheng, G.; Wang, X.; Hu, X.; Ding, X. Photocatalytic degradation of mixed gaseous carbonyl compounds at low level on adsorptive TiO₂/SiO₂ photocatalyst using a fluidized bed reactor. *Chemosphere* **2006**, *64*, 423–431. [[CrossRef](#)]
44. Zhang, Y.; Zhou, B.; Chen, H.; Yuan, R. Heterogeneous photocatalytic oxidation for the removal of organophosphorus pollutants from aqueous solutions: A review. *Sci. Total Environ.* **2023**, *856*, 159048. [[CrossRef](#)] [[PubMed](#)]
45. Cheikh, S.; Imessaoudene, A.; Bollinger, J.-C.; Hadadi, A.; Manseri, A.; Bouzaza, A.; Assadi, A.; Amrane, A.; Zamouche, M.; El Jery, A.; et al. Complete Elimination of the Ciprofloxacin Antibiotic from Water by the Combination of Adsorption–Photocatalysis Process Using Natural Hydroxyapatite and TiO₂. *Catalysts* **2023**, *13*, 336. [[CrossRef](#)]

Disclaimer/Publisher’s Note: The statements, opinions and data contained in all publications are solely those of the individual author(s) and contributor(s) and not of MDPI and/or the editor(s). MDPI and/or the editor(s) disclaim responsibility for any injury to people or property resulting from any ideas, methods, instructions or products referred to in the content.